

Accepted Manuscript

Calibration of a simple directional distortional hardening model for metal plasticity

Slavomír Parma, Jiří Plešek, René Marek, Zbyněk Hrubý,
Heidi P. Feigenbaum, Yannis F. Dafalias

PII: S0020-7683(18)30081-7
DOI: [10.1016/j.ijsolstr.2018.02.037](https://doi.org/10.1016/j.ijsolstr.2018.02.037)
Reference: SAS 9925



To appear in: *International Journal of Solids and Structures*

Received date: 6 December 2017

Accepted date: 16 February 2018

Please cite this article as: Slavomír Parma, Jiří Plešek, René Marek, Zbyněk Hrubý, Heidi P. Feigenbaum, Yannis F. Dafalias, Calibration of a simple directional distortional hardening model for metal plasticity, *International Journal of Solids and Structures* (2018), doi: [10.1016/j.ijsolstr.2018.02.037](https://doi.org/10.1016/j.ijsolstr.2018.02.037)

This is a PDF file of an unedited manuscript that has been accepted for publication. As a service to our customers we are providing this early version of the manuscript. The manuscript will undergo copyediting, typesetting, and review of the resulting proof before it is published in its final form. Please note that during the production process errors may be discovered which could affect the content, and all legal disclaimers that apply to the journal pertain.

Highlights

- A simple directional distortional hardening model is analytically integrated.
- Two calibration algorithms for model's parameters are proposed.
- Algorithms are suitable for both the monotonic and the cyclic loading modes.

Calibration of a simple directional distortional hardening model for metal plasticity

Slavomír Parma^{a,b}, Jiří Plešek^{a,*}, René Marek^a, Zbyněk Hrubý^a, Heidi P. Feigenbaum^c, Yannis F. Dafalias^d

^a*Institute of Thermomechanics of the Czech Academy of Sciences, Dolejšková 1402/5, 182 00 Prague, Czech Republic*

^b*Czech Technical University in Prague, Faculty of Mechanical Engineering, Technická 4, 166 07 Prague, Czech Republic*

^c*Northern Arizona University, Department of Mechanical Engineering, P.O. Box 15600, Flagstaff, AZ 86011, USA*

^d*University of California at Davis, Department of Civil and Environmental Engineering, Davis, CA 95616, USA*

^e*National Technical University of Athens, Faculty of Applied Mathematical and Physical Science, Zographou 15780, Greece*

Abstract

Directional distortional hardening (DDH) is the change of shape of the yield surface such that a region of high curvature develops roughly in the loading direction while a region of lower curvature develops in the opposite direction. In this paper, a simple model of DDH involving six material parameters is calibrated by analytical means. Analytical integration results in equations for the stress–strain curve, the hysteresis loop and the cyclic stress–strain curve inherent to the model. Based on these curves, two calibration procedures for model's parameters are proposed, and consequent analysis shows some basic properties of the model. The first calibration procedure is suited to model

*Corresponding author

Email address: plesek@it.cas.cz (Jiří Plešek)

URL: www.it.cas.cz (Jiří Plešek)

monotonic loading whereas the second one is suited to model cyclic loading cases.

Keywords: Plasticity, Hardening, Constitutive laws, Yield Surface, Calibration

1. Introduction

Distortion of yield surfaces due to strain hardening has been observed in numerous experiments on various types of metals, including but not limited to [Naghdi et al. \(1958\)](#), [McComb \(1960\)](#), [Phillips et al. \(1974\)](#), [Wu and Yeh](#)
 5 [\(1991\)](#), [Boucher et al. \(1995\)](#), [Ishikawa \(1997\)](#), and [Khan et al. \(2009\)](#). In stress space, the subsequent yield surfaces exhibit distorted ellipses, being highly curved in the direction of loading—often with a sharp apex—and flattened in the opposite direction.

Several complex mathematical models of distortional hardening were in-
 10 troduced in the last decades by [Ortiz and Popov \(1983\)](#), [Eisenberg and Yen \(1984\)](#), [Yen and Eisenberg \(1987\)](#), [Voyiadjis and Foroozesh \(1990\)](#), [Kurtyka and Życzkowski \(1996\)](#), [François \(2001\)](#), [Dafalias et al. \(2003\)](#), [Shutov et al. \(2011\)](#), and others.

[Feigenbaum and Dafalias \(2007, 2008\)](#) extended the work by [Dafalias](#)
 15 [et al. \(2003\)](#) introducing formally the notion of Directional Distortional Hardening (DDH). In their work, directional terms involving the trace of the product of unit norm deviatoric radial tensors with the backstress tensor were introduced in conjunction with two model concepts: one described in [Feigenbaum and Dafalias \(2007\)](#) utilizing the Armstrong–Frederick type equation
 20 for the evolution of fourth order tensor and the other proposed in [Feigenbaum and Dafalias \(2008\)](#) associated with fixed directional support in conjunction

with a second order tensor that can be chosen to be the backstress in the simplest case. The simplest model was implemented in a FE code by Marek et al. (2015).

25 Various problems arise with the identification of model parameters that are required to satisfy several constraints. Apart from thermodynamic constraints derived in the original papers by Feigenbaum and Dafalias (2007, 2008), conditions proved by Plešek et al. (2010) to guarantee convexity of distorted surfaces should be met so that the convergence of return mapping
30 numerical integrators is ensured Plešek and Kristek (1997) and the basic physics of crystal metal plasticity that demands convexity of yield surface is satisfied.

Despite the potential of simple trial and error fitting methods introduced in Feigenbaum (2008) to analyze essential features of the proposed models, there still remains a call for systematic approach to model's parameters
35 calibration. The distortion of the yield surface and the resulting strong non-linearity, in addition to kinematic and isotropic hardening, constitutes the main cause of such difficulties in calibration. In practice, the availability of such procedures is often a decisive factor in engineering preferences regarding
40 the choice of particular constitutive model.

It turns out that even for the simplest loading modes, such as the uniaxial tensile stress loading or pure shear stress loading, the reduced algebro-differential systems corresponding to majority of distortional hardening models are excessively complex not permitting analytical solutions. This, of
45 course, hinders finding a proper way to identify material parameters from tensile or torsion tests. This paper, nevertheless, shows that at least for one

of the models in Feigenbaum and Dafalias (2008) a close form solution exists and may be used for calibration purposes. The knowledge of such solution may also be used to check numerical integration algorithms or lend some
50 help for identification and analysis of more complex models supplying first approximation as well as general guidelines.

The text is organized as follows. Section 2 overviews the so-called α -model with fixed distortional parameter c , the simplest of the Feigenbaum and Dafalias directional distortional hardening models, including examples
55 of evolved yield surfaces and hardening curves. In Section 3, analytical solutions for fundamental load cases are provided. These solutions are followed in Section 4 by the proposal of a system of algebraic equations suitable for material parameters identification in terms of relatively simple load and unload stress-strain curves and distorted yield surfaces. Subsequently calibration is
60 presented based on cyclic stress-strain curves, where the material is cyclically loaded using strain control until a stable hysteresis loop is reached, then the maximum stress in the stable curve is plotted against the strain level. Satisfactory results are received for both approaches.

2. Constitutive model

The yield function f is based on the J_2 -invariant, which is subsequently modified by a directional multiplier as

$$f(\boldsymbol{\sigma}) = \frac{3}{2} [1 - c(\mathbf{n}_r : \boldsymbol{\alpha})] (\mathbf{s} - \boldsymbol{\alpha}) : (\mathbf{s} - \boldsymbol{\alpha}) - k^2 = 0, \quad (1)$$

where $\boldsymbol{\sigma}$ is the stress tensor; \mathbf{s} is the deviatoric stress tensor; $\boldsymbol{\alpha}$ is the deviatoric backstress tensor acting as the “center” of the yield surface; c is a

positive distortional parameter and k is a scalar internal variable. The double dot symbol represents the inner product of two tensors as in $\mathbf{a}:\mathbf{b} = a_{ij} b_{ij}$ and $\|\cdot\|$ denotes the Euclidean norm of a second order tensor. Further,

$$\mathbf{n}_r = \frac{\mathbf{s} - \boldsymbol{\alpha}}{\|\mathbf{s} - \boldsymbol{\alpha}\|} \quad (2)$$

65 is the deviatoric unit norm tensor along the radius $(\mathbf{s} - \boldsymbol{\alpha})$. Hence, it is the inner product $\mathbf{n}_r:\boldsymbol{\alpha}$ which is responsible for the directional distortion of the yield surface.

The model's internal variables are governed by standard evanescent memory type equations. The kinematic hardening rule is Armstrong–Frederick's type defined according to

$$\dot{\boldsymbol{\alpha}} = a_1 (\dot{\boldsymbol{\epsilon}}^p - a_2 \|\dot{\boldsymbol{\epsilon}}^p\| \boldsymbol{\alpha}), \quad (3)$$

and the isotropic hardening is defined by

$$\dot{k} = \lambda \kappa_1 k (1 - \kappa_2 k), \quad (4)$$

where λ is the loading index or plastic multiplier defined as usual in terms of stress or strain rate. Both of these evolution equations can be shown Feigenbaum and Dafalias (2008) to be sufficient to satisfy the second law of thermodynamics. Plastic strain rate is obtained by an associated flow rule

$$\dot{\boldsymbol{\epsilon}}^p = \lambda \frac{\partial f}{\partial \boldsymbol{\sigma}}. \quad (5)$$

The initial values are defined for unstrained material as $\boldsymbol{\epsilon}^p = \mathbf{0}$, $\boldsymbol{\alpha} = \mathbf{0}$ and $k = k_0$, that is, k_0 is the initial yield stress. Thus the model features six
70 positive parameters a_1 , a_2 , κ_1 , κ_2 , k_0 , and c . Details of this constitutive model are explained in Feigenbaum and Dafalias (2008).

In order to simplify governing equations, one can explicitly calculate the yield function gradient

$$\frac{\partial f}{\partial \boldsymbol{\sigma}} = \frac{3}{2} \|\mathbf{s} - \boldsymbol{\alpha}\| [2\mathbf{n}_r - c(\mathbf{n}_r : \boldsymbol{\alpha}) \mathbf{n}_r - c\boldsymbol{\alpha}] \quad (6)$$

and its magnitude as

$$\left\| \frac{\partial f}{\partial \boldsymbol{\sigma}} \right\| = \frac{3}{2} \|\mathbf{s} - \boldsymbol{\alpha}\| \sqrt{[2 - c(\mathbf{n}_r : \boldsymbol{\alpha})][2 - 3c(\mathbf{n}_r : \boldsymbol{\alpha})] + c^2 \boldsymbol{\alpha} : \boldsymbol{\alpha}}. \quad (7)$$

It was proved in [Feigenbaum and Dafalias \(2008\)](#) and [Plesek et al. \(2010\)](#) that the necessary and sufficient condition, which keeps dissipation positive and simultaneously preserves strict convexity for all times, yields

$$\|c\boldsymbol{\alpha}\| < 1. \quad (8)$$

Substitution of Eq. (5) into Eq. (3) yields

$$\dot{\boldsymbol{\alpha}} = a_1 \lambda \left\| \frac{\partial f}{\partial \boldsymbol{\sigma}} \right\| (\mathbf{n} - a_2 \boldsymbol{\alpha}). \quad (9)$$

For monotonic loading the saturated state is reached when $\dot{\boldsymbol{\alpha}} = \mathbf{0}$, thus, Eq. (9) yields

$$\mathbf{n} - a_2 \boldsymbol{\alpha} = \mathbf{0}. \quad (10)$$

Since $\boldsymbol{\alpha}$ starts from zero and the magnitude of the limit backstress, $1/a_2$, is independent of the loading direction, one may write

$$\|\boldsymbol{\alpha}\| \leq 1/a_2. \quad (11)$$

Hence the left-hand side of inequality (8) may be bounded by c/a_2 , which yields

$$c < a_2. \quad (12)$$

This is the only constraint to be observed in the present constitutive modeling.

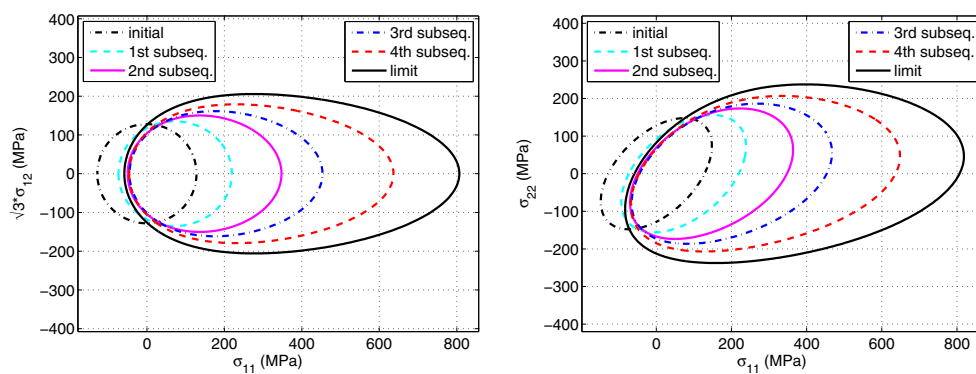


Figure 1: Yield loci evolution for stress driven loading

To illustrate the behavior of the discussed model, analytically derived
75 yield surfaces and stress-strain curves are shown in Figs. 1 and 2 using material parameters after Feigenbaum and Dafalias (2008), and given in Tab. 1. For this set of parameters, the condition stipulated by inequality (12) is fulfilled. The evolution of subsequent yield surfaces under uniaxial tension is shown in two stress subspaces in Fig. 1. Observe that all three kinds of hard-
80 ening, namely isotropic, kinematic and directional distortional, contribute to the plotted shapes of the yield surface. The stress-strain curves and the evolution of other internal variables are plotted in Fig. 2.

k_0	128 MPa
κ_1	6 000 MPa
κ_2	0.006 MPa ⁻¹
a_1	10 500 MPa
a_2	0.02 MPa ⁻¹
c	0.019 MPa ⁻¹

Table 1: Parameters after Feigenbaum and Dafalias (2008).

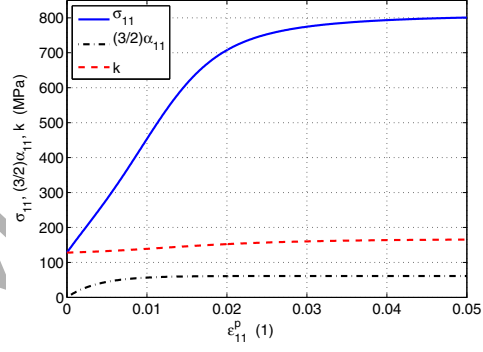


Figure 2: Evolution of stress and internal variables for parameters from Tab. 1. The σ_{11} curve represents a stress-strain curve in $\sigma_{11} - \epsilon_{11}^p$ variables.

3. Closed form solutions in simple loading modes

In this section, the closed form solution of the stress-strain curve for
 85 uniaxial tensile loading in the 1 direction and the distorted yield surface is
 derived as well as the analytical solution for the corresponding cyclic stress-
 strain curve. These analytical solutions may serve as a check on numerical
 integration algorithms, or as we will show in subsequent sections as a means
 to calibrate the model. Furthermore, these analytic solutions may help pro-
 90 vide an initial guess for purely numerical calibration schemes, particularly
 when more complex versions of these models are used.

3.1. Proportional loading/unloading

Using Eqs. (3), (4), and (5), and expressing the loading index λ in terms
 of the uniaxial plastic strain rate, the rate forms for kinematic and isotropic
 hardening under uniaxial loading can be expressed as follows:

$$\dot{\alpha}_{11} = a_1 \dot{\epsilon}_{11}^p \left(1 - m \sqrt{\frac{3}{2}} a_2 \alpha_{11} \right), \quad (13)$$

$$\dot{k} = \kappa_1 (1 - \kappa_2 k) \frac{m \dot{\epsilon}_{11}^p}{\sqrt{1 - m \sqrt{\frac{3}{2}} c \alpha_{11}}}, \quad (14)$$

where the symbol m is used to identify the loading direction, with $m = 1$ for
 loading towards tension and $m = -1$ for loading towards compression.

After some algebra, that can be found in Appendix A, Eqs. (13) and (14)
 yield by integration

$$\alpha_{11} = \sqrt{\frac{2}{3}} \frac{1}{m a_2} \left[1 - \left(1 - m \sqrt{\frac{3}{2}} a_2 \alpha_{11,0} \right) \cdot \exp \left(-m \sqrt{\frac{3}{2}} a_1 a_2 (\epsilon_{11}^p - \epsilon_{11,0}^p) \right) \right] \quad (15)$$

and

$$k = \frac{1}{\kappa_2} [1 - (1 - \kappa_2 k_0) \cdot \exp \xi], \quad (16)$$

where

$$\xi = -\sqrt{\frac{2}{3}} \frac{\kappa_1 \kappa_2}{a_1 \sqrt{a_2(a_2 - c)}} (\tanh^{-1}(1/p) - \tanh^{-1}(1/p_0)),$$

$$p(\epsilon_{11}^p) = \sqrt{1 + \frac{c}{a_2 - c} \left(1 - m \sqrt{\frac{3}{2}} a_2 \alpha_{11,0}\right) \exp\left(-m \sqrt{\frac{3}{2}} a_1 a_2 (\epsilon_{11}^p - \epsilon_{11,0}^p)\right)},$$

$$p_0 = p(\epsilon_{11,0}^p) = \sqrt{1 + \frac{c}{a_2 - c} \left(1 - m \sqrt{\frac{3}{2}} a_2 \alpha_{11,0}\right)},$$

respectively. The following two initial conditions were used in the above equations:

$$\alpha_{11,0} = \alpha_{11}(\epsilon_{11,0}^p), \quad (17)$$

$$k_0 = k(\epsilon_{11,0}^p). \quad (18)$$

95 In general, the initial axial plastic strain $\epsilon_{11,0}^p$ can be arbitrary. To model the stress-strain curve of a virgin material, however, the loading starts from zero plastic strain and zero backstress, i.e., $\epsilon_{11,0}^p = 0$ and $\alpha_{11,0} = 0$, and the yield stress k_0 remains a general material parameter which needs to be calibrated from experiment.

Finally, the stress tensor component σ_{11} can be expressed from Eq. (1) as

$$\sigma_{11} = \frac{mk}{\sqrt{1 - m \sqrt{\frac{3}{2}} c \alpha_{11}}} + \frac{3}{2} \alpha_{11}, \quad (19)$$

100 where terms α_{11} and k are governed by Eqs. (15) and (16), respectively.

Once the virgin material is uniaxially prestrained, the yield condition Eq. (1) under subsequent biaxial stress loading becomes

$$f(\sigma_{11}, \sigma_{12}) = \left[1 - c \frac{3 \left(\frac{\sigma_{11}}{3} - \frac{\alpha_{11}}{2} \right) \alpha_{11}}{\sqrt{6 \left(\frac{\sigma_{11}}{3} - \frac{\alpha_{11}}{2} \right)^2 + \frac{2}{3} (\sqrt{3} \sigma_{12})^2}} \right] \left[6 \left(\frac{\sigma_{11}}{3} - \frac{\alpha_{11}}{2} \right)^2 + \frac{2}{3} (\sqrt{3} \sigma_{12})^2 \right] - \frac{2}{3} k^2 \leq 0, \quad (20)$$

where α_{11} and k are values of internal variables evolved by uniaxial prestraining and given by Eqs. (15) and (16), respectively, and σ_{11} and σ_{12} are the stress tensor components defining the biaxial stress state.

3.2. Cyclic stress-strain curve

Under strain controlled cyclic loading, the locus of vertices of the stabilized stress-strain hysteresis loops obtained for different amplitudes of plastic strain constitutes the so called cyclic stress-strain curve (CSSC). Specifically how CSSC is found from stabilized stress-strain hysteresis loops is shown Fig. 3.

Eq. (16) implies that the isotropic hardening variable k monotonically evolves along any plastic straining path and reaches its limit value $k_{\text{lim}} = 1/\kappa_2$. Thus, in case of uniaxial cyclic loading the isotropic hardening is saturated after several cycles and does not evolve anymore. Eq. (15) implies that the backstress component α_{11} alternates under uniaxial cyclic straining. Following an approach by [Lemaitre and Chaboche \(1990\)](#), it is assumed that backstress component α_{11} forms a closed symmetric hysteresis loop. It is proved in [Appendix B](#), that this assumption is valid for the backstress given

by Eq. (15). After some algebra that can also be found in [Appendix B](#), the backstress amplitudes are obtained in the form

$$\alpha_{11,a} = \sqrt{\frac{2}{3}} \frac{1}{a_2} \tanh \left(\sqrt{\frac{3}{2}} a_1 a_2 \epsilon_{11,a}^p \right), \quad (21)$$

where $\epsilon_{11,a}^p$ is the plastic strain component amplitude. Hereafter, the amplitude refers to the peak amplitude that is a half of peak-to-peak amplitude of variable respective. Thus, Eq. (21) describes “cyclic backstress–strain curve.” The cyclic stress–strain curve then can be obtained from Eqs. (19) and (21) in the form

$$\sigma_{11,a} = \frac{1/\kappa_2}{\sqrt{1 - \frac{c}{a_2} \tanh \left(\sqrt{\frac{3}{2}} a_1 a_2 \epsilon_{11,a}^p \right)}} + \sqrt{\frac{3}{2}} \frac{1}{a_2} \tanh \left(\sqrt{\frac{3}{2}} a_1 a_2 \epsilon_{11,a}^p \right), \quad (22)$$

where $\sigma_{11,a}$ is the stress component amplitude evoked by the plastic strain component amplitude $\epsilon_{11,a}^p$. Since the isotropic hardening variable k is saturated, the initial parameter k_0 and rate parameter κ_1 do not figure in Eq. (22) and the set of model’s parameters describing the CSSC is reduced to four independent considerable parameters κ_2 , a_1 , a_2 , and c .

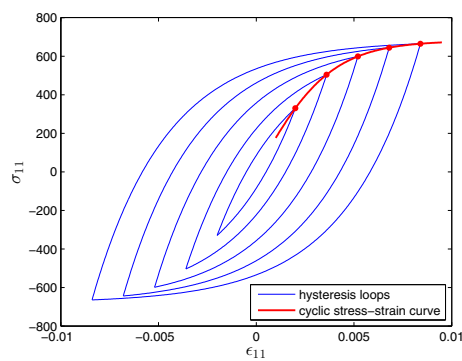


Figure 3: Example of how a particular cyclic stress-strain curve (CSSC) is constructed from subsequent stabilized hysteresis loops.

115 4. Calibration procedures

Two independent calibration procedures for model's parameters are proposed. The first one is suited to calibrate parameters based on monotonic loading data for corresponding monotonic loading simulations. This procedure reflects distortion of the yield surface, stress-strain diagram and some
 120 reversals in loading and uses these experimental data as an input. Moreover, the calibration procedure allows one to determinate model's parameters by analytical solution of a system of several nonlinear equations.

The other procedure calibrates parameters from experimental cyclic stress-strain curve data. Parameters obtained by this procedure are suitable to
 125 model cyclic loading cases. This second calibration method is based on the nonlinear least squares problem formulation and requires a numerical solver. The nonlinear methods require a good initial estimate of parameters to satisfy convergence of the algorithm, and the closed form solution from the previous section helps provide this estimation.

130 4.1. Proportional loading/unloading

In general, the proposed calibration procedure requires 10 experimental inputs that are shown in the Figs. 4–7 and denoted A_1, \dots, D_3 . These experimental inputs can be expressed as a function of model's parameters in the form $\{A_1, \dots, D_3\} = \mathcal{F}(k_0, \kappa_1, \kappa_2, a_1, a_2, c)$. A closed form analytical in-
 135 version of this system will be shown and model's parameters are formally expressed by $\{k_0, \kappa_1, \kappa_2, a_1, a_2, c\} = \mathcal{F}^{-1}(A_1, \dots, D_3)$.

In particular, the calibration procedure is based on parametric approximation of 4 experimental curves, which serve as inputs. The first experi-

mental curve is set to be the stress-strain curve as shown in Fig. 4. This
 140 experimental input is referred to as the A experiment. The second experi-
 mental curve is set to be the stress-strain curve with a reversal of loading
 at some level $\epsilon_{11,B}^P$ of plastic strain. This diagram is shown in Fig. 5 and is
 referred to as the B experiment. The third experimental curve is set to be
 the stress-strain curve with a reversal of loading at some different level $\epsilon_{11,C}^P$
 145 of plastic strain. This diagram is shown in Fig. 6 and is referred to as the
 C experiment. The difference between the B and C experiments is in the
 plastic strain levels. Further in this text, it is shown that strain levels $\epsilon_{11,B}^P$
 and $\epsilon_{11,C}^P$ denoting the loading reversal have to satisfy the specific condition
 $\epsilon_{11,C}^P/\epsilon_{11,B}^P = 2$ to provide a closed form calibration. The fourth experimental
 150 curve is set to be the distorted yield surface in $\sigma_{11}-\sqrt{3}\sigma_{12}$ subspace obtained
 for arbitrary uniaxial plastic prestrain. This curve is shown in Fig. 7 and
 is referred to as the D experiment. Although tracing of distorted surfaces
 is quite complex and rather expensive, it is quite common in experimen-
 tal research of plasticity as can be seen in Wu and Yeh (1991); Ishikawa
 155 (1997); among others. Moreover, there are modern testing systems that are
 able to do this experiment autonomously as reported in Sung et al. (2011).
 Thus, four experiments denoted A, B, C and D will be used for calibration of
 aforementioned six parameters $k_0, \kappa_1, \kappa_2, a_1, a_2$, and c . It is possible to cover
 experiments A, B, C and even D on a single specimen. This can be done if
 160 the reversals at plastic strain levels $\epsilon_{11,B}^P$ and $\epsilon_{11,C}^P$ in experiments B and C
 and the probing of the yield surface in experiment D do not cause significant
 plastic strain or mutually influence the individual experiments.

As the derivation of the calibration algorithm is relatively long, it is in-

cluded in [Appendix C](#). Equations following in the rest of this section form
165 the calibration algorithm itself without any more detailed explanation.

Having experimentally determined 10 input parameters A_1 , A_2 , A_3 , B_1 ,
 B_2 , C_1 , C_2 , D_1 , D_2 , and D_3 , the parameters of model can be obtained as
follows.

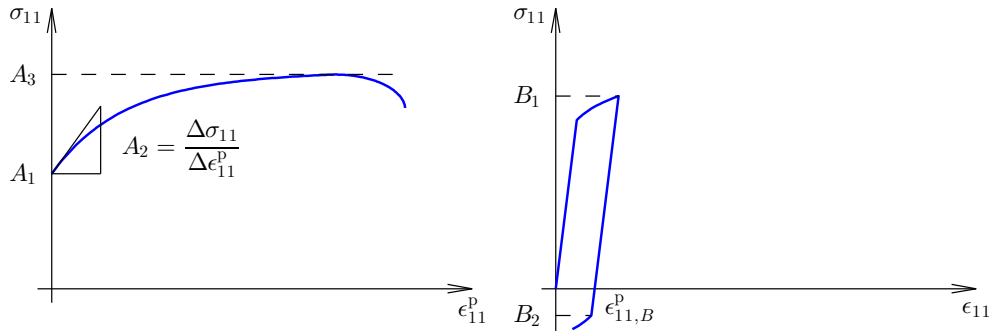


Figure 4: Stress-strain curve data—the A experiment.

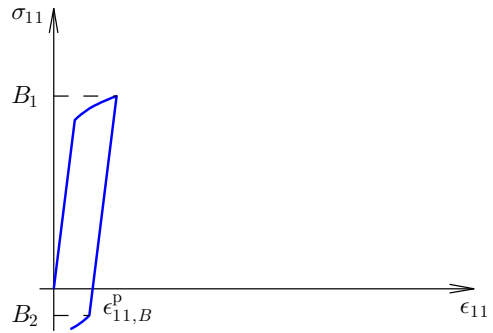


Figure 5: Reversal loading data—the B experiment.

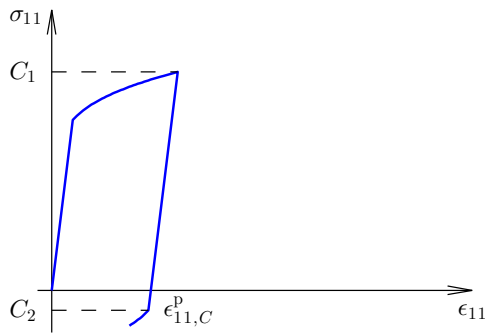


Figure 6: Reversal loading data—the C experiment.

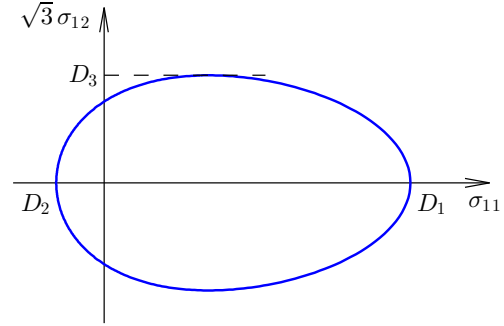


Figure 7: Shape of the distorted surface—the D experiment.

The k_0 parameter results from the A experiment and can be expressed as

$$k_0 = A_1. \quad (23)$$

The c parameter, which is associated with yield surface distortion arises from the D experiment, which shows the yield surface shape, as:

$$c = \frac{3 \cdot \sqrt{(D_1 - D_2)(D_1 - D_2 - 2D_3)}}{(D_1 - D_2 - D_3) \left[D_1 + D_2 - \sqrt{(D_1 - D_2)(D_1 - D_2 - 2D_3)} \right]}. \quad (24)$$

As can be seen from Fig. 7, the term $D_1 - D_2 - 2D_3$ in Eq. (24) represents the difference between the length and the width of the evolved yield surface at the experiment D. Since the term under the square root in Eq. (24) must be positive, Eq. (24) implies that the length of the yield surface at the D experiment must be larger than the width of this surface. It should be emphasized that Eq. (24) expresses an inherent property of the DDH model itself and thus has a significant impact on the model properties. In general, the equation implies that for any value of model's parameter c the yield surface elongates in the straining direction and shrinks in the transverse direction, which contradicts various experimental results, e.g., Phillips et al. (1974), Wu and Yeh (1991) and Ishikawa (1997). Because this property of the model contradicts some experimental findings, it is undesirable, but cannot be eliminated in the current model. Furthermore, the square root at the denominator of Eq. (24) implies that experimental parameters are also constrained by relation $D_3 \geq -2D_1D_2/(D_1 - D_2)$.

The a_2 parameter can be determined on the basis of the B and C experiments. First, the backstress values $\alpha_{11,B}$ and $\alpha_{11,C}$ on two levels of plastic

deformation $\epsilon_{11,B}^p$ and $\epsilon_{11,C}^p$ respectively need to be expressed. The backstress α_{11} ($\epsilon_{11,B}^p$) on some level of plastic deformation $\epsilon_{11,B}^p$ can be expressed as

$$\alpha_{11,B} = -\frac{L}{3K} - \frac{1}{3K} \sqrt[3]{\frac{1}{2} \left[2L^3 - 9KLM + 27K^2N + \sqrt{-27K^2\Delta} \right]} - \frac{1}{3K} \sqrt[3]{\frac{1}{2} \left[2L^3 - 9KLM + 27K^2N - \sqrt{-27K^2\Delta} \right]}, \quad (25)$$

where Δ is defined as

$$\Delta = 18KLMN - 4L^3N + L^2M^2 - 4KM^3 - 27K^2N^2, \quad (26)$$

and

$$K = \frac{9}{2} \sqrt{\frac{3}{2}} c, \quad L = -3 \sqrt{\frac{3}{2}} c (B_1 + B_2), \quad (27)$$

$$M = \sqrt{\frac{3}{2}} c (B_1^2 + B_2^2) + 3(B_1 - B_2), \quad N = -(B_1^2 - B_2^2). \quad (28)$$

It should be noted that Eq. (25) is valid under the condition $B_2 < 0$. For
 185 more details, see the [Appendix C](#).

The $\alpha_{11,C}$ backstress can be expressed in the same way substituting for the B experiment parameters the C experiment parameters. Finally, the a_2 parameter can be expressed as

$$a_2 = \sqrt{\frac{2}{3}} \frac{2\alpha_{11,B} - \alpha_{11,C}}{\alpha_{11,B}^2}. \quad (29)$$

Note that this equation assumes that $\epsilon_{11,C}^p / \epsilon_{11,B}^p = 2$.

Having the a_2 parameter, the a_1 parameter can be written in the form

$$a_1 = -\sqrt{\frac{2}{3}} \frac{1}{a_2 \epsilon_{11,B}^p} \ln \left(1 - \sqrt{\frac{3}{2}} \alpha_{11,B} a_2 \right). \quad (30)$$

Further, the κ_2 parameter may be expressed as

$$\kappa_2 = \frac{1}{\sqrt{1 - \frac{c}{a_2}} \cdot \left(A_3 - \sqrt{\frac{3}{2}} \frac{1}{a_2} \right)}. \quad (31)$$

Finally, the κ_1 parameter can be written in form

$$\kappa_1 = \frac{2A_2 - \sqrt{\frac{3}{2}} k_0 a_1 c - 3a_1}{1 - \kappa_2 k_0}. \quad (32)$$

Thus, all material parameters are calibrated.

In order to present a calibration example, an experimental data is necessary. However, the authors have no experimental data available and data in the literature generally do not include all necessary experiments for calibration. Moreover, experiments in the literature, e.g., [Phillips et al. \(1974\)](#), [Wu and Yeh \(1991\)](#) and [Ishikawa \(1997\)](#), show shortening of the yield surface in the direction of loading, while this model requires elongation in the direction of loading. Thus, the calibration example in this work utilizes data generated by the model itself.

Material parameters from Tab. 1 were used to generate the 4 “experimental” plots similar to that ones in Figs. 4–7. From these plots, experimental parameters were read of and summarized in Tab. 2. Thus, Tab. 2 should be thought of as a simulation of experiments. Then, using the identification algorithm in Eqs. (23)–(32), the experimental parameters from Tab. 2 give the model parameters in Tab. 3.

Figs. 8 and 9 compare the original stress–strain curves and yield surfaces obtained with the assumed parameters in Tab. 1 to those obtained for identified parameters in Tab. 3. The original and identified stress–strain curves

205 as well as the original and identified yield surfaces show good agreement. Furthermore, the parameters in Tab. 1 and Tab. 3 are similar. All of this suggest that the identification algorithm in Eqs. (23)–(32) provides sufficient accuracy.

In order to test a robustness of the calibration algorithm, some intentional errors in reading from generated experimental data were introduced. Thus, 210 there is about 5% difference in the data in Tab. 2 and exact values gained from parameters in Tab. 1. As can be seen in Figs. 8 and 9, these intentional errors do not evoke an essential deviation between the original and calibrated model in terms of generated curves. On the other hand, as can be seen from 215 Tabs. 1 and 3, there can be an essential deviation between the original and calibrated internal parameters of the model. This property of the calibration algorithm is supposed to be related to the sensitivity of model's parameters relatively to experimental data. Therefore, the sensitivity analysis of calibration algorithm has been performed and is described in Section 4.3. If no 220 intentional errors are involved and exact reading is performed, calibration algorithm fully recovers original parameters and graphs matches exactly.

A_1	126 MPa
A_2	30674 MPa
A_3	805 MPa
B_1	449 MPa
B_2	-47 MPa
C_1	706 MPa
C_2	-51 MPa
D_1	382 MPa
D_2	-47 MPa
D_3	155 MPa
$\epsilon_{11,B}^p$	1 %
$\epsilon_{11,C}^p$	2 %
$\epsilon_{11,D}^p$	0.8 %

Table 2: Experimental parameters obtained from plots generated using the model parameters in Tab. 1.

k_0	126.00 MPa
κ_1	2880.9 MPa
κ_2	0.0063571 MPa ⁻¹
a_1	9349.1 MPa
a_2	0.023718 MPa ⁻¹
c	0.022684 MPa ⁻¹

Table 3: Calibrated model parameters.

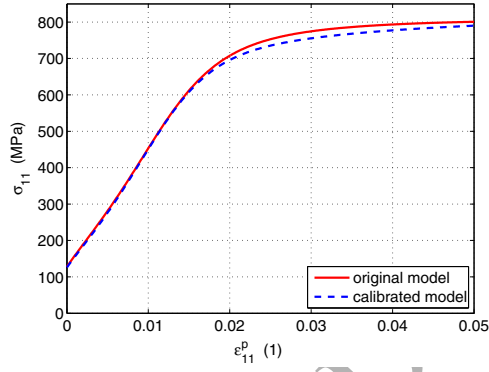


Figure 8: Original and identified stress-strain curves comparison.

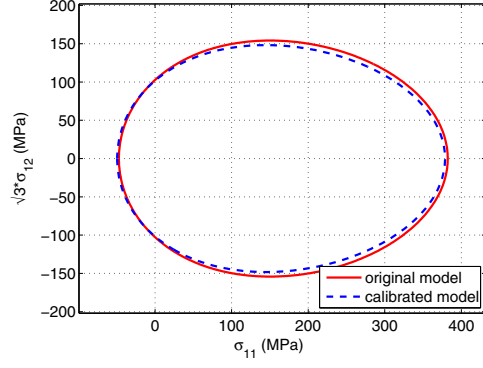


Figure 9: Comparison of distorted yield surfaces of the original and identified model.

4.2. Cyclic stress–strain curve

Several experimental parameters can be determined from experimental cyclic stress–strain curve (CSSC). Referring to Fig. 10, the P parameter denotes an initial size of the elastic domain. The R parameter denotes the limit size of elastic domain. Finally, the Q parameter denotes the stress amplitude for arbitrary plastic strain amplitude $\epsilon_{11,a,Q}^p$. Because the stress amplitude must increase as strain amplitude increases, $P < Q < R$. For practical application, the experimental parameter P can be determined as the minimal stress amplitude of the experimental CSSC, the parameter R can be determined as the maximum stress amplitude of the experimental CSSC, and the parameter Q can be determined as the stress amplitude at plastic strain amplitude $\epsilon_{11,a,Q}^p$, where $\epsilon_{11,a,Q}^p$ is any plastic strain amplitude of the experimental CSSC. Note better results are obtained if Q is selected near the middle between P and R in terms of stress. Using Eq. (22), parameters P , Q , and R can be related to the model's parameters. The P parameter can be expressed by setting $\epsilon_{11,a}^p = 0$ in Eq. (22) as

$$P = \sigma_{11,a} (\epsilon_{11,a}^p \rightarrow 0_+) = \frac{1}{\kappa_2}. \quad (33)$$

The stress amplitude Q at some level of plastic strain amplitude $\epsilon_{11,a,Q}^p$ can be expressed as

$$Q = \sigma_{11,a} (\epsilon_{11,a,Q}^p) = \frac{1/\kappa_2}{\sqrt{1 - \frac{c}{a_2} \tanh \left(\sqrt{\frac{3}{2}} a_1 a_2 \epsilon_{11,a,Q}^p \right)}} + \sqrt{\frac{3}{2}} \frac{1}{a_2} \tanh \left(\sqrt{\frac{3}{2}} a_1 a_2 \epsilon_{11,a,Q}^p \right). \quad (34)$$

Further, the limit value R of function (22) can be expressed by setting $\epsilon_{11,a}^P \rightarrow +\infty$ in Eq. (22) as

$$R = \sigma_{11,a} (\epsilon_{11,a}^P \rightarrow +\infty) = \frac{1}{\kappa_2} \frac{1}{\sqrt{1 - \frac{c}{a_2}}} + \sqrt{\frac{3}{2}} \frac{1}{a_2}. \quad (35)$$

The ratio of the c and the a_2 parameters can be defined as r , i.e.,

$$r = \frac{c}{a_2}. \quad (36)$$

In Eqs. (33)–(36), parameters P , Q and R can be determined from experimental data. Due to the restrictions $0 \leq c < a_2$, that can be seen in Feigenbaum and Dafalias (2008), Eqs. (33), (35), and (36) yield

$$R = P \frac{1}{\sqrt{1-r}} + \sqrt{\frac{3}{2}} \frac{1}{a_2} > P \frac{1}{\sqrt{1-r}}. \quad (37)$$

The inequality (37) imposes an restriction on the r parameter that can be expressed as

$$0 \leq r < 1 - \left(\frac{P}{R} \right)^2. \quad (38)$$

Sensitivity analysis of the DDH model with respect to the c parameter shows that higher values of the r parameter are necessary to make the c parameter significant in terms of CSSC influence. Different CSSCs for different values of the r parameter and fixed parameters P , Q and R can be seen in Fig. 11.

In this figure, the fixed parameters P , Q and R cause that all depicted curves have a common original point, a cross point and a limit value, respectively.

Note that influence of r is small. Thus, the r parameter can be estimated as 90 % of the upper limit value given by Eq. (38). This estimation yields

$$r = 0.9 \left(1 - (P/R)^2 \right). \quad (39)$$

Once the left hand sides of Eqs. (33)–(36) are determined, system of four nonlinear equations for four parameters is formulated. Solution of this system
225 gives the initial estimation for material parameters a_1 , a_2 , κ_2 and c .

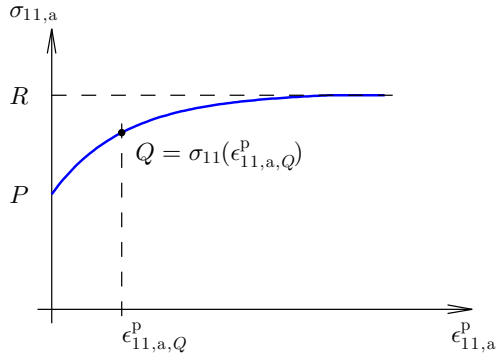


Figure 10: Geometrical representation of experimental parameters P , Q and R .

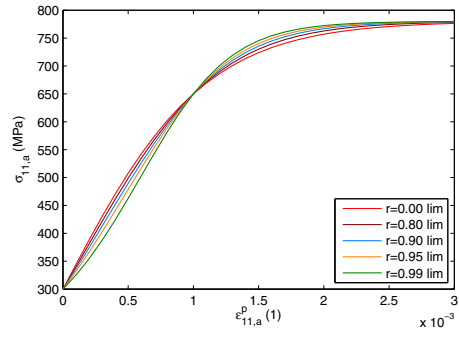


Figure 11: Different CSSC for different values of the parameter r and fixed values of parameters P , Q and R .

Although the system of Eqs. (33)–(36) is nonlinear, some equations can be solved in analytical way. Thus, Eq. (33) yields

$$\kappa_2 = \frac{1}{P}, \quad (40)$$

Eq. (35) yields

$$a_2 = \frac{\sqrt{\frac{3}{2}}}{R - \frac{P}{\sqrt{1-r}}} \quad (41)$$

and Eq. (36) yields

$$c = ra_2. \quad (42)$$

Further, substituting solutions (40) and (41) into Eq. (34) one obtains relation

$$f(a_1) = 0, \quad (43)$$

where

$$f(a_1) = \frac{P}{\sqrt{1 - r \tanh\left(\frac{\frac{3}{2}\epsilon_{11,a,Q}^p}{R - \frac{P}{\sqrt{1-r}}}a_1\right)}} + \left(R - \frac{P}{\sqrt{1-r}}\right) \tanh\left(\frac{\frac{3}{2}\epsilon_{11,a,Q}^p}{R - \frac{P}{\sqrt{1-r}}}a_1\right) - Q. \quad (44)$$

Eq. (43) involves only one unknown variable a_1 and can be solved very effectively by numerical means.

In order to show the existence and uniqueness of a solution, the function in Eq. (44) has been analyzed. The only restriction for the a_1 parameter is

$a_1 \geq 0$, as can be seen in [Feigenbaum and Dafalias \(2008\)](#). It can be easily shown that

$$f(a_1)|_0 = P - Q < 0, \quad (45)$$

and

$$\lim_{a_1 \rightarrow +\infty} f(a_1) = R - Q > 0, \quad (46)$$

that guaranties the existence of solution in $[0, +\infty)$. Because for $a_1 \geq 0$,

$$f'(a_1) > 0, \quad (47)$$

uniqueness of solution in $[0, +\infty)$ is guarenteed as well. To solve Eq. (43) the bisection method was used. The left endpoint for the first iteration of the
 230 bisection method can be choosen as $a_1 = 0$, the right one can be determined by trivial algorithm based on Eq. (46).

304LN		AISI 1018 HR				
total strain	stress	total strain	stress			
amplitude	amplitude	amplitude	amplitude			
(%)	(MPa)	(%)	(MPa)			
0.20	256	0.13	207		304LN	AISI 1018 HR
0.50	312	0.26	253	P	256 MPa	207 MPa
0.77	354	0.39	272	Q	430.5 MPa	305.5 MPa
1.00	403	0.52	287	R	583 MPa	355 MPa
1.20	458	0.65	299	r	0.72647	0.59400
1.40	491	0.78	312	$\epsilon_{14a,Q}^P$	0.88475 %	0.56225 %
1.60	531	0.91	323			
1.80	563	1.04	334			
2.00	583	1.17	345			
		1.30	355			

Table 4: Experimental data of cyclic stress-strain curves for steels 304LN Paul et al. (2011) and AISI 1018 HR Plumtree and Abdel-Raouf (2001).

Table 5: Parameters estimated from the experimental data in Tab. 4.

	304LN	AISI 1018 HR
κ_2	0.0040199 MPa ⁻¹	0.0046638 MPa ⁻¹
a_1	2.8795 MPa	135.30 MPa
a_2	0.33586 MPa ⁻¹	0.0083313 MPa ⁻¹
c	0.28411 MPa ⁻¹	1.7763e-9 MPa ⁻¹

Table 6: Parameters of model identified from the experimental data in Tab. 4 using non-linear least squares method. An initial estimation of model's parameters was obtained using Eqs. (40)–(43) and data from Tab. 5.

In order to present a calibration example, experimental data of CSSC after Paul et al. (2011) and Plumtree and Abdel-Raouf (2001) was taken. Data is summarized in Tab. 4 and depicted in Figs. 12 and 13. Because no
235 elastic moduli of materials in Paul et al. (2011) and Plumtree and Abdel-Raouf (2001) were given, Young's modulus of both materials was estimated to be $E = 2 \times 10^5$ MPa.

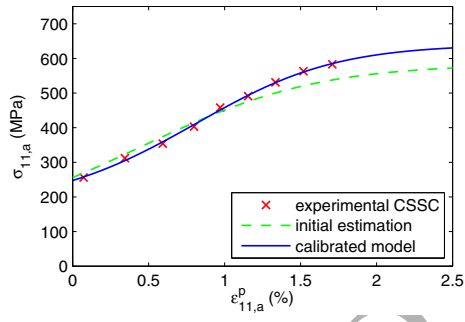


Figure 12: Model calibrated on 304LN experimental data.

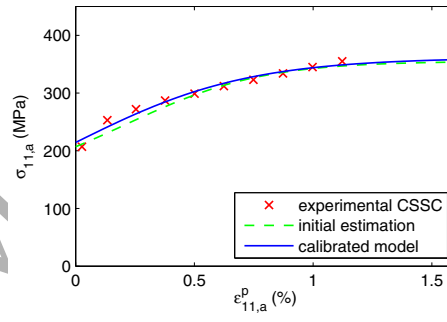


Figure 13: Model calibrated on AISI 1018 HR experimental data.

Identification of DDH model on experimental data of CSSC can be performed by the Least Squares Method (LSM). However, because the model Eq. (22) is nonlinear to its parameters, nonlinear formulation of the LSM have to be used. In order to obtain a good initial estimation of parameters, an identification algorithm based on Eqs. (40)–(43) can be used for this estimation and final identification can be performed by the nonlinear LSM.

Two examples from model performance after initial estimation and final identification are shown in Figs. 12 and 13 and appropriate parameters of model are summarized in Tab. 6.

4.3. Sensitivity analysis of calibration procedures

In order to understand relations between inputs and outputs of calibration procedures and to test robustness of these procedures, a sensitivity analysis of both procedures was carried out. The approach is to consider the derivative $\partial p_{\text{int}}/\partial P_{\text{inp}}$ of a model internal parameter p_{int} with respect to an input data P_{inp} , and pre-multiply it by $P_{\text{inp}}/p_{\text{int}}$ for normalization. In general, since inputs of calibration algorithms are experimentally determined and can be represented as mechanical properties of modeled material, the sensitivity analysis of calibration procedures reveals sensitivity of model's parameters to some basic mechanical properties of modeled material, e.g., the yield strength and the ultimate tensile strength.

For the sensitivity analysis of monotonic calibration algorithm given by Eqs. (23)–(32), parameters from Tab. 2 were used. The sensitivity matrix is given by

$$\begin{pmatrix}
 \frac{A_1}{k_0} \frac{\partial k_0}{\partial A_1} & \frac{A_2}{k_0} \frac{\partial k_0}{\partial A_2} & \frac{A_3}{k_0} \frac{\partial k_0}{\partial A_3} & \frac{B_1}{k_0} \frac{\partial k_0}{\partial B_1} & \frac{B_2}{k_0} \frac{\partial k_0}{\partial B_2} & \frac{C_1}{k_0} \frac{\partial k_0}{\partial C_1} & \frac{C_2}{k_0} \frac{\partial k_0}{\partial C_2} & \frac{D_1}{k_0} \frac{\partial k_0}{\partial D_1} & \frac{D_2}{k_0} \frac{\partial k_0}{\partial D_2} & \frac{D_3}{k_0} \frac{\partial k_0}{\partial D_3} \\
 \frac{A_1}{\kappa_1} \frac{\partial \kappa_1}{\partial A_1} & \frac{A_2}{\kappa_1} \frac{\partial \kappa_1}{\partial A_2} & \frac{A_3}{\kappa_1} \frac{\partial \kappa_1}{\partial A_3} & \frac{B_1}{\kappa_1} \frac{\partial \kappa_1}{\partial B_1} & \frac{B_2}{\kappa_1} \frac{\partial \kappa_1}{\partial B_2} & \frac{C_1}{\kappa_1} \frac{\partial \kappa_1}{\partial C_1} & \frac{C_2}{\kappa_1} \frac{\partial \kappa_1}{\partial C_2} & \frac{D_1}{\kappa_1} \frac{\partial \kappa_1}{\partial D_1} & \frac{D_2}{\kappa_1} \frac{\partial \kappa_1}{\partial D_2} & \frac{D_3}{\kappa_1} \frac{\partial \kappa_1}{\partial D_3} \\
 \frac{A_1}{\kappa_2} \frac{\partial \kappa_2}{\partial A_1} & \frac{A_2}{\kappa_2} \frac{\partial \kappa_2}{\partial A_2} & \frac{A_3}{\kappa_2} \frac{\partial \kappa_2}{\partial A_3} & \frac{B_1}{\kappa_2} \frac{\partial \kappa_2}{\partial B_1} & \frac{B_2}{\kappa_2} \frac{\partial \kappa_2}{\partial B_2} & \frac{C_1}{\kappa_2} \frac{\partial \kappa_2}{\partial C_1} & \frac{C_2}{\kappa_2} \frac{\partial \kappa_2}{\partial C_2} & \frac{D_1}{\kappa_2} \frac{\partial \kappa_2}{\partial D_1} & \frac{D_2}{\kappa_2} \frac{\partial \kappa_2}{\partial D_2} & \frac{D_3}{\kappa_2} \frac{\partial \kappa_2}{\partial D_3} \\
 \frac{A_1}{a_1} \frac{\partial a_1}{\partial A_1} & \frac{A_2}{a_1} \frac{\partial a_1}{\partial A_2} & \frac{A_3}{a_1} \frac{\partial a_1}{\partial A_3} & \frac{B_1}{a_1} \frac{\partial a_1}{\partial B_1} & \frac{B_2}{a_1} \frac{\partial a_1}{\partial B_2} & \frac{C_1}{a_1} \frac{\partial a_1}{\partial C_1} & \frac{C_2}{a_1} \frac{\partial a_1}{\partial C_2} & \frac{D_1}{a_1} \frac{\partial a_1}{\partial D_1} & \frac{D_2}{a_1} \frac{\partial a_1}{\partial D_2} & \frac{D_3}{a_1} \frac{\partial a_1}{\partial D_3} \\
 \frac{A_1}{a_2} \frac{\partial a_2}{\partial A_1} & \frac{A_2}{a_2} \frac{\partial a_2}{\partial A_2} & \frac{A_3}{a_2} \frac{\partial a_2}{\partial A_3} & \frac{B_1}{a_2} \frac{\partial a_2}{\partial B_1} & \frac{B_2}{a_2} \frac{\partial a_2}{\partial B_2} & \frac{C_1}{a_2} \frac{\partial a_2}{\partial C_1} & \frac{C_2}{a_2} \frac{\partial a_2}{\partial C_2} & \frac{D_1}{a_2} \frac{\partial a_2}{\partial D_1} & \frac{D_2}{a_2} \frac{\partial a_2}{\partial D_2} & \frac{D_3}{a_2} \frac{\partial a_2}{\partial D_3} \\
 \frac{A_1}{c} \frac{\partial c}{\partial A_1} & \frac{A_2}{c} \frac{\partial c}{\partial A_2} & \frac{A_3}{c} \frac{\partial c}{\partial A_3} & \frac{B_1}{c} \frac{\partial c}{\partial B_1} & \frac{B_2}{c} \frac{\partial c}{\partial B_2} & \frac{C_1}{c} \frac{\partial c}{\partial C_1} & \frac{C_2}{c} \frac{\partial c}{\partial C_2} & \frac{D_1}{c} \frac{\partial c}{\partial D_1} & \frac{D_2}{c} \frac{\partial c}{\partial D_2} & \frac{D_3}{c} \frac{\partial c}{\partial D_3}
 \end{pmatrix} = \begin{pmatrix}
 1.00000 & 0 & 0 & 0 & 0 & 0 & 0 & 0 & 0 & 0 \\
 -53.059 & 107.01 & -4.3008 & -137.86 & 69.738 & 55.864 & -25.794 & 2.2324 & 1.6481 & -5.4739 \\
 0 & 0 & -1.0685 & -0.34747 & 0.15309 & 1.2597 & -0.58165 & 0.58165 & 0.42939 & -1.4262 \\
 0 & 0 & 0 & 1.2873 & -0.56716 & -0.47916 & 0.22124 & -0.75347 & -0.55624 & 1.8475 \\
 0 & 0 & 0 & 0.031483 & -0.013871 & -0.11414 & 0.052701 & 1.3397 & 0.98901 & -3.2849 \\
 0 & 0 & 0 & 0 & 0 & 0 & 0 & 1.4011 & 1.0343 & -3.4354
 \end{pmatrix}. \quad (48)$$

This analysis reveals higher sensitivity of the internal rate parameter κ_1 to experimental parameters A_1, \dots, D_3 , while other internal parameters have rather lower sensitivity.

For the sensitivity analysis of cyclic calibration algorithm given by Eqs. (40)–(43), parameters from Tab. 5 of the 304LN grade steel were used. The sensitivity matrix is given by

$$\begin{pmatrix} \frac{P}{\kappa_2} \frac{\partial \kappa_2}{\partial P} & \frac{Q}{\kappa_2} \frac{\partial \kappa_2}{\partial Q} & \frac{R}{\kappa_2} \frac{\partial \kappa_2}{\partial R} & \frac{r}{\kappa_2} \frac{\partial \kappa_2}{\partial r} \\ \frac{P}{a_1} \frac{\partial a_1}{\partial P} & \frac{Q}{a_1} \frac{\partial a_1}{\partial Q} & \frac{R}{a_1} \frac{\partial a_1}{\partial R} & \frac{r}{a_1} \frac{\partial a_1}{\partial r} \\ \frac{P}{a_2} \frac{\partial a_2}{\partial P} & \frac{Q}{a_2} \frac{\partial a_2}{\partial Q} & \frac{R}{a_2} \frac{\partial a_2}{\partial R} & \frac{r}{a_2} \frac{\partial a_2}{\partial r} \\ \frac{P}{c} \frac{\partial c}{\partial P} & \frac{Q}{c} \frac{\partial c}{\partial Q} & \frac{R}{c} \frac{\partial c}{\partial R} & \frac{r}{c} \frac{\partial c}{\partial r} \end{pmatrix} = \begin{pmatrix} -1.00000 & 0 & 0 & 0 \\ -5.3719 & 2.6687 & 3.6820 & -5.2944 \\ 5.2342 & 0 & -6.2342 & 6.9507 \\ 5.2342 & 0 & -6.2342 & 7.9507 \end{pmatrix}. \quad (49)$$

This analysis reveals low sensitivity of all internal model's parameters to experimental parameters P , Q , R and r . Suggesting that the model and calibration procedure is rather robust and slight changes to the selected experimental parameters yields only small changes to predicted results.

5. Concluding remarks

In order to supply satisfactory phenomenological description of the effects of directional distortional hardening, the mathematical model [Feigenbaum and Dafalias \(2008\)](#) was proposed. The presented work established analytic solutions and calibration procedures for the α -model with constant parameter c , which has six independent material parameters. Besides this, a detailed analysis of model revealed some advantages and drawbacks of model.

The first of two calibration procedures proposed in this paper is based on evaluating of key features of stress–strain curves experimentally obtained under uniaxial stress loading with some loading reversals, and on the measured

shape of the evolved yield surface shape in $\sigma_{11}-\sqrt{3}\sigma_{12}$ space, as a representative of the biaxial behavior. These points include initial yield stress, slope, strength, yield stresses under reversals, and dimensions of the evolved
 280 shape of yield surface. They can be represented analytically via the governing equations of the model, forming a system of **six** nonlinear equations for six unknown model's parameters. This solution can be obtained in a closed form, i.e., without using numerical methods or iterative approximations.

285 The second calibration algorithm proposed in this paper employs cyclic stress-strain curve to calibrate model's parameters. The algorithm consists of two steps. In the first step, the parameters are estimated based on rough approximation of this curve. In the second step, a nonlinear least squares formulation is used to fit the analytical model of the CSSC to experimental
 290 data. Within this step, the initial estimation of parameters obtained from the first step is used. Here it should be emphasized, that model allows one to capture an inflection in the CSSC, as can be seen in Fig. 12. This behavior makes this DDH model suitable for modeling cyclic loading modes.

However, it should be noted, that analysis of model preceding the calibration algorithm development showed some limitations of the model itself.
 295 This limitation arises from Eq. (24). The equation implies that distorted surfaces generated by model are more elongated in the straining direction than in the direction perpendicular to the straining. However, this behavior contradicts some experimental observations that show substantial shrinking of
 300 yield surface dimension in the straining direction suggesting that this model is not ideal to capture unloading cases and the need for a new DDH model.

With a new model, new closed form solutions would be needed, but the general

calibration procedures outlined in this work could still be used.

Acknowledgements

305 This work was supported by the Ministry of Education, Youth and Sports of the Czech Republic [grant numbers KONTAKT II LH14018, CENDYN-MAT CZ.02.1.01/0.0/0.0/15_003/0000493]; and the Czech Science Foundation [grant number GAČR 15-20666].

References

310 Boucher, M., Cayla, P., Cordebois, J. P., 1995. Experimental studies of yield surfaces of aluminium alloy and low carbon steel under complex biaxial loading. *European Journal of Mechanics – A/Solids* 14 (1), pp. 1–17.

Dafalias, Y. F., Schick, D., Tsakmakis, C., 2003. A simple model for describing yield surface evolution during plastic flow. In: Hutter, K., Baaser, H. (Eds.), *Deformation and Failure in Metallic Materials. Lecture Notes in Applied and Computational Mechanics*. Springer Berlin Heidelberg, pp. 169–201.

URL http://dx.doi.org/10.1007/978-3-540-36564-8_7

Eisenberg, M. A., Yen, C.-F., 1984. The anisotropic deformation of yield surfaces. *Journal of Engineering Materials and Technology* 106 (4), pp. 355–360.

320 URL <http://dx.doi.org/10.1115/1.3225730>

Feigenbaum, H. P., 2008. Directional distortional hardening in plasticity

based on thermodynamics. PhD dissertation, University of California,
 325 Davis.

Feigenbaum, H. P., Dafalias, Y. F., 2007. Directional distortional hardening
 in metal plasticity within thermodynamics. *International Journal of Solids
 and Structures* 44 (4), pp. 22–23.

URL [http://www.sciencedirect.com/science/article/pii/
 330 S0020768307002077](http://www.sciencedirect.com/science/article/pii/S0020768307002077)

Feigenbaum, H. P., Dafalias, Y. F., 2008. Simple model for directional
 distortional hardening in metal plasticity within thermodynamics. *Journal
 of Engineering Mechanics* 134 (9), pp. 730–738.

URL [http://ascelibrary.org/doi/abs/10.1061/%28ASCE%
 335 290733-9399%282008%29134%3A9%28730%29](http://ascelibrary.org/doi/abs/10.1061/%28ASCE%290733-9399%282008%29134%3A9%28730%29)

François, M., 2001. A plasticity model with yield surface distortion for
 non proportional loading. *International Journal of Plasticity* 17 (5),
 pp. 703–717.

URL [http://www.sciencedirect.com/science/article/pii/
 340 S0749641900000255](http://www.sciencedirect.com/science/article/pii/S0749641900000255)

Ishikawa, H., 1997. Subsequent yield surface probed from its current center.
International Journal of Plasticity 13 (6–7), pp. 533–549.

URL [http://www.sciencedirect.com/science/article/pii/
 S0749641997000247](http://www.sciencedirect.com/science/article/pii/S0749641997000247)

345 Khan, A. S., Kazmi, R., Pandey, A., Stoughton, T., 2009. Evolution of
 subsequent yield surfaces and elastic constants with finite plastic deforma-

tion. Part-I: A very low work hardening aluminum alloy (Al6061-T6511).
International Journal of Plasticity 25 (9), pp.1611–1625, exploring New
Horizons of Metal Forming Research.

350 URL [http://www.sciencedirect.com/science/article/pii/
S0749641908001113](http://www.sciencedirect.com/science/article/pii/S0749641908001113)

Kurtyka, T., Życzkowski, M., 1996. Evolution equations for distortional
plastic hardening. International Journal of Plasticity 12 (2), pp. 191–213.

URL [http://www.sciencedirect.com/science/article/pii/
355 S0749641996000034](http://www.sciencedirect.com/science/article/pii/S0749641996000034)

Lemaitre, J., Chaboche, J.-L., 1990. Mechanics of Solid Materials. Cambridge
University Press.

Marek, R., Plešek, J., Hrubý, Z., Parma, S., Feigenbaum, H. P., Dafalias,
Y. F., 2015. Numerical implementation of a model with directional distortional
360 hardening. Journal of Engineering Mechanics, pp.04015048 .

URL [http://dx.doi.org/10.1061/\(ASCE\)EM.1943-7889.0000954](http://dx.doi.org/10.1061/(ASCE)EM.1943-7889.0000954)

McComb, H. G., 1960. Some experiments concerning subsequent yield surfaces in plasticity. Tech. Rep. D-396, National Aeronautics and Space Administration.

365 Naghdi, P. M., Essenburg, F., Koff, W., 1958. Experimental study of initial
and subsequent yield surface in plasticity. Journal of Applied Mechanics
201 (25), pp. 201–209.

Ortiz, M., Popov, E. P., 1983. Distortional hardening rules for metal plasticity. Journal of Engineering Mechanics 109 (4), pp. 1042–1057.

- 370 Paul, S. K., Sivaprasad, S., Dhar, S., Tarafder, S., 2011. Key issues in cyclic plastic deformation: Experimentation. *Mechanics of Materials* 43 (11), pp. 705–720.
URL <http://www.sciencedirect.com/science/article/pii/S0167663611001347>
- 375 Phillips, A., Tang, J.-L., Ricciuti, M., 1974. Some new observations on yield surfaces. *Acta Mechanica* 20 (1–2), pp. 23–39.
URL <http://dx.doi.org/10.1007/BF01374960>
- Pleseck, J., Feigenbaum, H. P., Dafalias, Y. F., 2010. Convexity of yield surface with directional distortional hardening rules. *Journal of Engineering*
380 *Mechanics* 136 (4), pp. 477–484.
- Pleseck, J., Kristek, A., 1997. Assessments of methods for locating the point of initial yield. *Computer Methods in Applied Mechanics and Engineering* 141 (3–4), pp. 389–397.
URL <http://www.sciencedirect.com/science/article/pii/S004578259601122X>
385
- Plumtree, A., Abdel-Raouf, H. A., 2001. Cyclic stress–strain response and substructure. *International Journal of Fatigue* 23 (9), pp. 799–805.
URL <http://www.sciencedirect.com/science/article/pii/S0142112301000378>
- 390 Shutov, A. V., Panhans, S., Kreissig, R., 2011. A phenomenological model of finite strain viscoplasticity with distortional hardening.

ZAMM-ZEITSCHRIFT FÜR ANGEWANDTE MATHEMATIK UND
MECHANIK 91 (8), pp. 653–680.

395 Sung, S., Liu, L., Hong, H., Wu, H., 2011. Evolution of yield surface in the
2D and 3D stress spaces. International Journal of Solids and Structures
48 (6), pp. 1054–1069.
URL [http://www.sciencedirect.com/science/article/pii/
S0020768310004476](http://www.sciencedirect.com/science/article/pii/S0020768310004476)

Voyiadjis, G. Z., Foroozesh, M., 1990. Anisotropic distortional yield model.
400 Computer Methods in Applied Mechanics and Engineering 57 (3), pp. 537–
547.
URL <http://dx.doi.org/10.1115/1.2897056>

Wu, H. C., Yeh, W. C., 1991. On the experimental determination of yield
surfaces and some results on annealed 304 stainless steel. International
405 Journal of Plasticity 7 (8), pp. 803–826.
URL [http://www.sciencedirect.com/science/article/pii/
074964199190019U](http://www.sciencedirect.com/science/article/pii/074964199190019U)

Yen, C. F., Eisenberg, M. A., 1987. The role of a loading surface in viscoplas-
ticity theory. Acta Mechanica 69 (1–4), pp. 77–96.
410 URL <http://dx.doi.org/10.1007/BF01175715>

Appendix A. Analytical integration for the uniaxial stress loading mode.

Assuming uniaxial loading mode and using relations (1) and (5), Eqs. (3) and (4) for evolution of α and k respectively can be expressed as

$$\dot{\alpha}_{11} = a_1 \dot{\epsilon}_{11}^p \left(1 - a_2 \sqrt{\frac{3}{2}} \alpha_{11} \operatorname{sgn}(s_{11} - \alpha_{11}) \right), \quad (\text{A1})$$

$$\dot{k} = \kappa_1 (1 - \kappa_2 k) \frac{\dot{\epsilon}_{11}^p \operatorname{sgn}(s_{11} - \alpha_{11})}{\sqrt{1 - c \sqrt{\frac{3}{2}} \operatorname{sgn}(s_{11} - \alpha_{11}) \alpha_{11}}}. \quad (\text{A2})$$

Henceforth, the term $\operatorname{sgn}(s_{11} - \alpha_{11})$ will be denoted as m . Using the relation

$$\frac{dg}{dt} = \frac{dg}{d\epsilon_{11}^p} \frac{d\epsilon_{11}^p}{dt} \quad (\text{A3})$$

Eqs. (A1) and (A2) emerge to their final form as

$$\alpha'_{11} = a_1 \left(1 - m \sqrt{\frac{3}{2}} a_2 \alpha_{11} \right), \quad (\text{A4})$$

$$k' = \frac{1}{2} \frac{m \kappa_1 (1 - \kappa_2 k)}{\sqrt{1 - m \sqrt{\frac{3}{2}} c \alpha_{11}}}, \quad (\text{A5})$$

where $(.)'$ operator is defined by $(.)' \equiv d(.) / d\epsilon_{11}^p$. The initial condition for Eq. (A4) can be written as

$$\alpha_{11}(\epsilon_{11,0}^p) = \alpha_{11,0} \quad (\text{A6})$$

and for Eq. (A5) as

$$k(\epsilon_{11,0}^p) = k_0. \quad (\text{A7})$$

It should be emphasized that not every initial condition $\{\epsilon_{11,0}^p, \alpha_{11,0}, k_0\}$ is admissible. Initial condition for variable α should fulfill inequality (11), and for the variable k similar restriction can be established. The integration of Eqs. (A4) and (A6) can be obtain in the form

$$\alpha_{11} = \sqrt{\frac{2}{3}} \frac{1}{m a_2} \left[1 - \left(1 - m \sqrt{\frac{3}{2}} a_2 \alpha_{11,0} \right) \cdot \exp \left(-m \sqrt{\frac{3}{2}} a_1 a_2 (\epsilon_{11}^p - \epsilon_{11,0}^p) \right) \right]. \quad (\text{A8})$$

The integration of Eqs. (A5) and (A7) can be found using the separation of variables method. To find integral

$$\int \frac{m \cdot d\epsilon_{11}^p}{\sqrt{1 - m \sqrt{\frac{3}{2}} c \alpha_{11}}}, \quad (\text{A9})$$

that arises in algebraic operations, substitutions $m \sqrt{\frac{3}{2}} c \alpha_{11} = \varphi$, $\sqrt{1 - \varphi} = p$, and $\sqrt{\frac{a_2}{a_2 - c}} p = q$ can be used. Finally, the solution can be obtained in the form

$$k = \frac{1}{\kappa_2} [1 - (1 - \kappa_2 k_0) \cdot \exp \xi], \quad (\text{A10})$$

where

$$\begin{aligned} \xi &= -\sqrt{\frac{2}{3}} \frac{\kappa_1 \kappa_2}{a_1 \sqrt{a_2 (a_2 - c)}} (\tanh^{-1}(p) - \tanh^{-1}(p_0)), \\ p(\epsilon_{11}^p) &= \sqrt{1 + \frac{c}{a_2 - c} \left(1 - m \sqrt{\frac{3}{2}} a_2 \alpha_{11,0} \right) \exp \left(-m \sqrt{\frac{3}{2}} a_1 a_2 (\epsilon_{11}^p - \epsilon_{11,0}^p) \right)}, \\ p_0 = p(\epsilon_{11,0}^p) &= \sqrt{1 + \frac{c}{a_2 - c} \left(1 - m \sqrt{\frac{3}{2}} a_2 \alpha_{11,0} \right)}. \end{aligned}$$

Thus, relations (A8) and (A10) express the evolution of α_{11} and k respectively. Finally, the stress tensor component σ_{11} can be expressed from Eq. (1). The given expression is

$$\sigma_{11} = \frac{mk}{\sqrt{1 - m\sqrt{\frac{3}{2}}c\alpha_{11}}} + \frac{3}{2}\alpha_{11}. \quad (\text{A11})$$

Substituting Eqs. (A8) and (A10) into the Eq. (A11) one obtains relation between the stress and the strain for a general monotonic uniaxial stress loading mode. The stress-strain curve equation can be obtained using relation (A11) and following specific (initial) conditions: $m = 1$, $\epsilon_{11,0}^p = 0$, $\alpha_{11}(\epsilon_{11,0}^p) = 0$, $k(\epsilon_{11,0}^p) = k_0$.

Appendix B. Analytical solution for the cyclic stress-strain curve (CSSC)

The cyclic stress-strain curve is a locus of vertices of the stabilized stress-strain hysteresis loops generated by strain controlled cyclic loading and obtained for different amplitudes of strain as shown in Fig. 3. To derive an equation of the cyclic stress-strain curve, the same technique as in Lemaitre and Chaboche (1990) is used. Note, however, before an equation for the CSSC can be derived, it must be first shown that backstress forms a closed symmetric hysteresis loop.

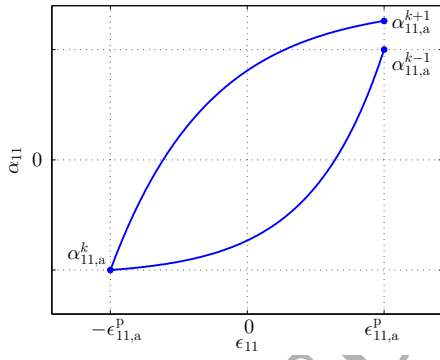


Figure B.14: A sequence of backstress loading steps.

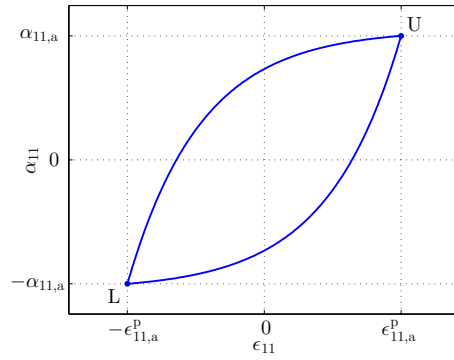


Figure B.15: Symmetric hysteresis loop for backstress.

Let's suppose that a uniaxial symmetric cyclic strain loading with the strain amplitude $\epsilon_{11,a}$ occurs. A backstress response to such a loading can be seen in Fig. B.14. Eq. (15) implies that after the k -th loading step—let's suppose that this loading step is compressive—the backstress amplitude is given by

$$\alpha_{11,a}^k = -\sqrt{\frac{2}{3}} \frac{1}{a_2} \left[1 - \left(1 + \sqrt{\frac{3}{2}} a_2 \alpha_{11,a}^{k-1} \right) \cdot \exp \left(-\sqrt{\frac{3}{2}} a_1 a_2 (2\epsilon_{11,a}^p) \right) \right], \quad (\text{B1})$$

where $\alpha_{11,a}^{k-1}$ is an initial condition from the previous loading step. After the subsequent $(k+1)$ step—which is tensile—the backstress amplitude is given by

$$\alpha_{11,a}^{k+1} = \sqrt{\frac{2}{3}} \frac{1}{a_2} \left[1 - \left(1 - \sqrt{\frac{3}{2}} a_2 \alpha_{11,a}^k \right) \cdot \exp \left(-\sqrt{\frac{3}{2}} a_1 a_2 (2\epsilon_{11,a}^p) \right) \right], \quad (\text{B2})$$

where $\alpha_{11,a}^k$ is an initial condition from the previous loading step. Denoting $\Delta_{k+1} = \alpha_{11,a}^{k+1} + \alpha_{11,a}^k$, one obtains

$$\begin{aligned} \Delta_{k+1} &= \exp \left(-\sqrt{\frac{3}{2}} a_1 a_2 (2\epsilon_{11,a}^p) \right) (\alpha_{11,a}^k + \alpha_{11,a}^{k-1}) \\ &= \exp \left(-\sqrt{\frac{3}{2}} a_1 a_2 (2\epsilon_{11,a}^p) \right) \Delta_k. \end{aligned} \quad (\text{B3})$$

Since $\exp \left(-\sqrt{\frac{3}{2}} a_1 a_2 (2\epsilon_{11,a}^p) \right) < 1$, the sequence Δ_k is a convergent geometric sequence and $\lim_{k \rightarrow +\infty} \Delta_k = 0$. Thus, limit value $\alpha_{11,a}^{k-1} + \alpha_{11,a}^k \xrightarrow{k \rightarrow +\infty} 0$ implies that $\alpha_{11,a}^{k-1} \xrightarrow{k \rightarrow +\infty} -\alpha_{11,a}^k$ and therefore the vertices of hysteresis loop are symmetric. Moreover, it can be easily shown that relation $\alpha_{11,a}^{k-1} \xrightarrow{k \rightarrow +\infty} \alpha_{11,a}^{k+1}$ also holds and therefore the hysteresis loop is closed, eventually as shown in Fig. B.15.

Eq. (15) implies that the isotropic hardening variable k is saturated due to the cyclic character of loading and therefore the backstress α remains the only evolving internal variable. Thus, a closed stabilized stress-strain hysteresis loop is conditioned by a closed stabilized hysteresis loop for α_{11} . To obtain a closed symmetric hysteresis loop for α_{11} , its vertices must meet conditions

$$L = \begin{pmatrix} -\epsilon_{11,a}^p & -\alpha_{11,a} \end{pmatrix}, \quad (B4)$$

$$U = \begin{pmatrix} \epsilon_{11,a}^p & \alpha_{11,a} \end{pmatrix}, \quad (B5)$$

where L and U are the lower and upper vertices of the loop, respectively, $\epsilon_{11,a}^p$ is the plastic strain amplitude and $\alpha_{11,a}$ is the backstress amplitude, as shown in Fig. B.15. Since the backstress evolves from the L vertex to the U vertex, Eq. (15) yields

$$\alpha_{11,a} = \sqrt{\frac{2}{3}} \frac{1}{a_2} \left[1 - \left(1 - \sqrt{\frac{3}{2}} a_2 \alpha_{11,a} \right) \cdot \exp \left(-\sqrt{\frac{3}{2}} a_1 a_2 2 \epsilon_{11,a}^p \right) \right]. \quad (B6)$$

From this equation, the backstress amplitude can be obtained in the form

$$\alpha_{11,a} = \sqrt{\frac{2}{3}} \frac{1}{a_2} \tanh \left(\sqrt{\frac{3}{2}} a_1 a_2 \epsilon_{11,a}^p \right), \quad (B7)$$

where $\epsilon_{11,a}^p$ is the plastic strain amplitude. The cyclic stress-strain curve then can be obtained from Eqs. (19) and (B7) in the form

$$\sigma_{11,a} = \frac{1/\kappa_2}{\sqrt{1 - \frac{c}{a_2} \tanh \left(\sqrt{\frac{3}{2}} a_1 a_2 \epsilon_{11,a}^p \right)}} + \sqrt{\frac{3}{2}} \frac{1}{a_2} \tanh \left(\sqrt{\frac{3}{2}} a_1 a_2 \epsilon_{11,a}^p \right). \quad (B8)$$

Appendix C. Derivation of identification algorithm and appropriate equations.

The starting point of plastic part of stress-strain curve is determined by the relation

$$A_1 = \sigma_{11}(\epsilon_{11}^p) \big|_{\epsilon_{11}^p=0} = \sigma_Y = k_0. \quad (C1)$$

At the start of the plastic part of the stress-strain curve the slope can be expressed as

$$A_2 = \frac{\partial \sigma_{11}}{\partial \epsilon_{11}^p}(\epsilon_{11}^p) \big|_{\epsilon_{11}^p=0} = \frac{1}{2} \kappa_1 (1 - \kappa_2 k_0) + \frac{1}{2} \sqrt{\frac{3}{2}} k_0 a_1 c + \frac{3}{2} a_1. \quad (C2)$$

If plastic deformation ϵ_{11}^p is fully developed, one can suppose that limit state is reached, i.e.,

$$A_3 = \lim_{\epsilon_{11}^p \rightarrow +\infty} \sigma_{11}(\epsilon_{11}^p) = \frac{1}{\kappa_2} \frac{1}{\sqrt{1 - \frac{c}{a_2}}} + \sqrt{\frac{3}{2}} \frac{1}{a_2}. \quad (C3)$$

From Eq. (19) flows, that the yield stress in tensile direction (\oplus) at some ($\epsilon_{11,B}^p$) level of plastic deformation can be expressed as

$$B_1 = \sigma_{11}(\epsilon_{11,B}^p)^\oplus = \frac{k(\epsilon_{11,B}^p)}{\sqrt{1 - \sqrt{\frac{3}{2}} \alpha_{11}(\epsilon_{11,B}^p) c}} + \frac{3}{2} \alpha_{11}(\epsilon_{11,B}^p). \quad (C4)$$

The yield stress in opposite direction (\ominus) at the same ($\epsilon_{11,B}^p$) level of plastic deformation can be expressed as

$$B_2 = \sigma_{11}(\epsilon_{11,B}^p)^\ominus = - \frac{k(\epsilon_{11,B}^p)}{\sqrt{1 + \sqrt{\frac{3}{2}} \alpha_{11}(\epsilon_{11,B}^p) c}} + \frac{3}{2} \alpha_{11}(\epsilon_{11,B}^p). \quad (C5)$$

The parametric expression of the C experiment is the same as in the previous case.

$$C_1 = \sigma_{11} (\epsilon_{11,C}^p)^\oplus = \frac{k (\epsilon_{11,C}^p)}{\sqrt{1 - \sqrt{\frac{3}{2}} \alpha_{11} (\epsilon_{11,C}^p) c}} + \frac{3}{2} \alpha_{11} (\epsilon_{11,C}^p) \quad (C6)$$

$$C_2 = \sigma_{11} (\epsilon_{11,C}^p)^\ominus = -\frac{k (\epsilon_{11,C}^p)}{\sqrt{1 + \sqrt{\frac{3}{2}} \alpha_{11} (\epsilon_{11,C}^p) c}} + \frac{3}{2} \alpha_{11} (\epsilon_{11,C}^p) \quad (C7)$$

Regarding the parametric description of the D experiment, the distorted yield surface in σ - $\sqrt{3}\tau$ space is shown on the Fig. 7. As significant points, the left, the right and the upper peak are choosen. This distorted surface is determined by Eq. (20). Analysing Eq. (20) the left and right peak of the distorted yield surface in σ - $\sqrt{3}\tau$ space can be expressed as

$$D_1 = \frac{k (\epsilon_{11,D}^p)}{\sqrt{1 - \sqrt{\frac{3}{2}} \alpha_{11} (\epsilon_{11,D}^p) c}} + \frac{3}{2} \alpha_{11} (\epsilon_{11,D}^p) \quad (C8)$$

$$D_2 = -\frac{k (\epsilon_{11,D}^p)}{\sqrt{1 + \sqrt{\frac{3}{2}} \alpha_{11} (\epsilon_{11,D}^p) c}} + \frac{3}{2} \alpha_{11} (\epsilon_{11,D}^p) \quad (C9)$$

This expression is possible if one declare $\sqrt{3}\tau = 0$ in Eq. (20). Further, the upper peak can be expressed in the form

$$D_3 = \sqrt{2}k (\epsilon_{11,D}^p) \frac{\sqrt{1 - \sqrt{1 - \frac{3}{2} \alpha_{11}^2 (\epsilon_{11,D}^p) c^2}}}{\sqrt{\frac{3}{2} \alpha_{11} (\epsilon_{11,D}^p) c}} \quad (C10)$$

435

The identification algorithm needs to determine six parameters of the model that depend on experimentally determined parameters A_1 , A_2 , A_3 ,

$B_1, B_2, B_3, C_1, C_2, C_3, D_1, D_2$ and D_3 . Parameters that must be identified are $k_0, a_1, a_2, \kappa_1, \kappa_2$ and c . The system of equations can be formulated for the determination of these parameters. The identification algorithm may
440 then be summarized as follows.

The k_0 parameter results from Eq. (C1). One can write

$$k_0 = A_1. \quad (C11)$$

The c parameter arises from Eqs. (C8), (C9) and (C10). This system can be solved analytically, the solution for the variable c is

$$c = \frac{3 \cdot \sqrt{(D_1 - D_2)(D_1 - D_2 - 2D_3)}}{(D_1 - D_2 - D_3) \left[D_1 + D_2 - \sqrt{(D_1 - D_2)(D_1 - D_2 - 2D_3)} \right]}. \quad (C12)$$

The a_2 parameter can be determined from the B and C experiments. At first, if one knows two values of the backstress α_{11} in Eq. (15), e.g., $\alpha_{11}(\epsilon_{11,B}^p)$ and $\alpha_{11}(\epsilon_{11,C}^p)$, apparently the a_2 parameter can be determined. Two values of the backstress $\alpha_{11}(\epsilon_{11,B}^p)$ and $\alpha_{11}(\epsilon_{11,C}^p)$ flows from Eqs. (C4), (C5) and (C6), (C7). The system (C4), (C5) leads to the cubic equation in form

$$K\alpha_{11,B}^3 + L\alpha_{11,B}^2 + M\alpha_{11,B} + N = 0, \quad (C13)$$

where

$$K = \frac{9}{2}\sqrt{\frac{3}{2}}c, \quad L = -3\sqrt{\frac{3}{2}}c(B_1 + B_2), \quad (C14)$$

$$M = \sqrt{\frac{3}{2}}c(B_1^2 + B_2^2) + 3(B_1 - B_2), \quad N = -(B_1^2 - B_2^2). \quad (C15)$$

For this cubic equation, the discriminant can be written in form

$$\Delta = 18KLMN - 4L^3N + L^2M^2 - 4KM^3 - 27K^2N^2. \quad (C16)$$

It can be easily shown that for $B_2 < 0$, i.e., when plastic deformation in reversed direction occurs in compressive state, not in tensile one, $\Delta < 0$ and this equation has only one real solution. Moreover this solution can be expressed in form

$$\alpha_{11,B} = -\frac{L}{3K} - \frac{1}{3K} \sqrt[3]{\frac{1}{2} \left[2L^3 - 9KLM + 27K^2N + \sqrt{-27K^2\Delta} \right]} - \frac{1}{3K} \sqrt[3]{\frac{1}{2} \left[2L^3 - 9KLM + 27K^2N - \sqrt{-27K^2\Delta} \right]}, \quad (C17)$$

where no negative arguments occur in square roots. The $\alpha_{11,C}$ backstress can be expressed by the same way. Now, Eqs. (15) with initial condition $\alpha_{11,0} = 0$ can be rewritten into form

$$a_1 = -\sqrt{\frac{2}{3}} \frac{1}{a_2 \epsilon_{11,B}^p} \ln \left(1 - \sqrt{\frac{3}{2}} \alpha_{11,B} a_2 \right) \quad (C18)$$

for the $\epsilon_{11,B}^p$ level at reversion and into the form

$$a_1 = -\sqrt{\frac{2}{3}} \frac{1}{a_2 \epsilon_{11,C}^p} \ln \left(1 - \sqrt{\frac{3}{2}} \alpha_{11,C} a_2 \right) \quad (C19)$$

for the $\epsilon_{11,C}^p$ level at reversion. These two equations formulate a system that can be written in form

$$\left(1 - \sqrt{\frac{3}{2}} \alpha_{11,B} a_2 \right)^{\epsilon_{11,C}^p / \epsilon_{11,B}^p} + \sqrt{\frac{3}{2}} \alpha_{11,C} a_2 - 1 = 0. \quad (C20)$$

If the $\epsilon_{11,C}^p / \epsilon_{11,B}^p$ term equals 2, previous relation is a quadratic equation and its solution is

$$a_2 = \sqrt{\frac{2}{3}} \frac{2\alpha_{11,B} - \alpha_{11,C}}{\alpha_{11,B}^2}. \quad (C21)$$

Now the a_1 parameter flows from Eq. (C18). The κ_2 parameter flows from Eq. (C3) and can be expressed as

$$\kappa_2 = \frac{1}{\sqrt{1 - \frac{c}{a_2}} \left(A_3 - \sqrt{\frac{3}{2}} \frac{1}{a_2} \right)}. \quad (\text{C22})$$

Finally, the κ_1 parameter can be expressed from Eq. (C2) as

$$\kappa_1 = \frac{2A_2 - \sqrt{\frac{3}{2}} k_0 a_1 c - 3a_1}{1 - \kappa_2 k_0}. \quad (\text{C23})$$

Thus all parameters are determined.